Available online at www.sciencedirect.com

ScienceDirect

Energy Procedia 114 (2017) 1601 – 1614

Energy Procedia

13th International Conference on Greenhouse Gas Control Technologies, GHGT-13, 14-18 November 2016, Lausanne, Switzerland

CFD modeling of structured packings at small- and meso-scale

Daniel Sebastia-Saez[a,*], Sai Gu[a]

[a]*Dept. of Chemical and Process Engineering, University of Surrey, Stag Hill Campus, Guildford GU2 7XH, United Kingdom*

Abstract

This article presents a CFD model of the multiphase flow inside structured packings for amine-based post-combustion carbon capture. In the literature, simulations are performed at three scales due to computational limitations: small-, meso- and large-scale. This work focuses on small- and meso-scale, introducing interface tracking at both. The interfacial tracking is accomplished by using the Volume of Fluid (VoF) method. Small-scale allows studying the reaction kinetics of the absorption process in 2D geometries. Meso-scale has been used in the literature to describe the dry pressure drop of the packing (single-phase simulations). The interface tracking allows obtaining the relationship between the liquid load and both the liquid hold-up and the interface area. Data from the simulations are compared against experimental results found in the literature. The accurate modeling of the interface area, liquid hold-up and reaction kinetics allows utilizing this CFD model as a design tool for novel packings or to optimizing geometries already in use.

Peer-review under responsibility of the organizing committee of GHGT-13.

Keywords: CFD, structured packing, carbon capture and storage, post-combustion, interface tracking, Navier-Stokes equations, mass source term

1. Introduction

There is widespread consensus among the scientific community that using fossil fuels for power generation causes an increase in the concentration of greenhouse gases (GHGs) in the atmosphere. In fact, the concentration of carbon dioxide has risen from 280 ppm (pre-industrial level) to 385 ppm nowadays, which constitutes a substantial increase. Moreover, the growth rate is 2 ppm per annum, which means that the threshold established by world

* Corresponding author. Tel.: +44 (0) 7719 715575.
E-mail address: j.sebastiasaez@surrey.ac.uk

Peer-review under responsibility of the organizing committee of GHGT-13.
doi:10.1016/j.egypro.2017.03.1290

leaders (450 ppm) will be attained in the next few decades [1]. Nevertheless, energy is of paramount importance for industrial development and the increase in the population which the world is experiencing nowadays would not be possible without it. The concentration of carbon dioxide in the atmosphere should therefore be stabilized in order to avoid global warming and subsequent climate change. This could be achieved by switching from fossil fuels to other energy resources. However, only a limited number of energy resources would have enough potential to cover the current needs, being nuclear energy the most prominent among them. As of 2000, France, Japan and the U.S. covered 77%, 29%, and 20% of their energy needs respectively with nuclear energy despite concerns over nuclear waste disposal [2]. Conversely, renewable energies such as solar, tidal, wind, biomass, geothermal, and hydropower still have capacity limitations and can only compete against fossil fuels or nuclear power in a few instances, e.g. Iceland is a good example of the utilization of geothermal energy. The other feasible option nowadays is to continue using fossil fuels, yet implementing carbon capture and storage (CCS). Given the huge energy demand of modern society – which depends on a number of economic, social and political factors – and the theoretical capacity of the various energy resources available nowadays, it does not seem possible that fossil fuels could be abandoned in the near future.

In summary, the energy demand will continue increasing in the forthcoming decades and the world still has vast fossil fuel reserves available – particularly coal –, which cover 81% of the worldwide energy demand [3]. CCS acquires thus capital importance given the above context. The idea behind CCS is to store conveniently the same amount of carbon than that taken from the soil. There are three CCS technologies with a high potential of being implemented at the commercial scale: post-combustion, pre-combustion and oxy-combustion (also known as oxy-fuel), whilst technologies such as calcium looping are gaining importance in the last few years. Post-combustion CCS has the advantage that existing power plants could be retrofitted, since no significant modification in the power plant itself is required. In post-combustion CCS, carbon dioxide is removed from the flue gas after the combustion takes place conventionally. The facility consists of two columns: the absorber and the stripper. The flue gas from the power plant enters the absorber, i.e. a random or structured packed column, and comes into contact with a liquid absorbent, e.g. an aqueous amine solution. The output from the absorber is a clean gas stream ready to be emitted to the atmosphere and a CO_2-rich absorbent. The CO_2-rich solution is then retrieved in the stripper, where high temperatures are applied to break the bonds between the carbon and the absorbent. Residual heat from the steam cycle of the power plant itself is used to regenerate the absorbent. On the other hand, pre-combustion requires substantial modification of the existing facility because coal needs to undergo gasification before the combustion could take place. The gasification process renders a mixture of carbon monoxide and hydrogen. Shift reactions turn carbon monoxide into carbon dioxide and more hydrogen. The latter is separated from the stream and undergoes combustion, the sole product of which is water. Oxy-combustion also requires a significant modification on existing facilities. It consists in the combustion of the fuel in pure oxygen, which gives way to water and carbon dioxide as products. The main energy penalty in this technology is the separation of oxygen from air, which is an energy intensive process. Among the three options discussed, post-combustion has the highest potential to be implemented commercially. As a drawback, the implementation of CCS would result in an increase in the cost of power generation caused by the extra amount of energy needed to separate carbon dioxide from the flue gas. In the long-term however, the cost of carbon dioxide would overcome the operating costs and CCS would become commercially competitive. Once the carbon has been captured, it can be stored in suitable geological formations or used for commercial purposes. The latter include Enhanced Oil Recovery (EOR), Enhanced Gas Recovery (EGR) and Enhanced Coal Bed Methane Recovery (ECBM).

CFD is a useful tool to investigating the hydrodynamics of structured packings. However, due to computational resource limitations, the study needs to be divided into three scales: small-, meso-, and large-scale. Each scale focuses on some aspects of the flow. For example, small-scale simulations consist of small 2D or 3D computational domains with interface tracking. Raynal and Royan-Lebeaud established that small-scale is useful to visualize the flow over the surface texture of the structured packing [4]. One can thus obtain information on the reaction kinetics, the velocity at the gas-liquid interface and the liquid hold-up. The latter is an important parameter which affects the pressure drop of the packing, hence the importance of an accurate prediction. Meso-scale consists of single flow simulations inside the repeating unit which forms the geometry of the structured packing, i.e. the representative elementary unit or REU. The primary purpose of those calculations is to obtain the relationship between the gas superficial velocity and the pressure drop per unit length of the packing without the presence of the liquid phase –

dry pressure drop –. Estimations of the wet pressure drop can be obtained by correcting the gas superficial velocity with a factor which takes into account the presence of the liquid [5]. This factor modifies the porosity of the packing, since the presence of the liquid narrows the channels through which the gas flows. Finally, large-scale considers the whole column as a porous medium, allowing the analysis of liquid dispersion throughout the packing and the effect of geometric features within the absorber [6].

This paper shows the modelling work carried out so far in the field of structured packing columns for post-combustion CCS. The reactive mass transfer between the gas and the liquid phase within the structured packing column is described at small-scale. It also shows the capabilities of meso-scale when interface tracking methods are also included. The effect of flow parameters – such as viscosity and surface tension – on the liquid distribution over the packing is assessed. Further work will be directed towards the integration of the capabilities of the different modelling scales into more complete simulations.

2. Mathematical basis

2.1. Theoretical background and simulation set-up

The commercial software ANSYS-FLUENT v.14.0 is used to perform the calculations. The second order upwind spatial discretization scheme and the PRESTO algorithm for pressure correction are selected. The time step is set to be variable so as to keep the Courant number at a constant value of 0.5, which ensures the stability of the calculations. The VoF model is chosen to tracking the gas-liquid interface. The VoF model introduces a variable called volume fraction γ, the value of which varies between zero and one. The volume fraction field is obtained by solving an additional transport equation:

$$\frac{\partial \gamma}{\partial t} + \vec{v} \cdot \nabla \gamma = 0. \tag{1}$$

Once the volume fraction field is obtained, those cells the volume fraction of which is equal to one form the liquid phase whereas a value of zero means that they form the gas phase. Those cells which have a value of the volume fraction greater than zero and smaller than one form the interface. The VoF model solves the same set of conservation equations for both phases. This implies that the viscosity μ and the density ρ are not constant throughout the domain, but depend upon the volume fraction of both the gas and the liquid phase according to

$$\rho = \gamma_l \rho_l + \gamma_g \rho_g , \tag{2}$$

and

$$\mu = \gamma_l \mu_l + \gamma_g \mu_g , \tag{3}$$

where the subscripts l and g denote liquid and gas respectively.

The general mass balance over the differential volume would yield the following continuity equation, considering the mass source term S_{mass} which accounts for the reactive absorption:

$$\frac{\partial \rho}{\partial t} + \nabla \cdot \left(\rho \vec{v} \right) = S_{mass} . \tag{4}$$

Taking into account the variation of the density and the viscosity discussed above, Eqn. (4) can be developed further to obtain the following expression:

$$\frac{D\rho}{Dt}+\rho\left(\nabla\cdot\vec{v}\right)=S_{mass}. \tag{5}$$

As discussed hereafter, Eqn. (5) can be combined with the momentum conservation equation so as to obtain a single conservation expression which governs the present model.

The momentum conservation equation is obtained by adding all the forces which act on the fluid according to the expression

$$\sum\left(\vec{F}_{body}+\vec{F}_{surface}+\vec{F}_{additional}\right)=\left(-\nabla p+\mu\nabla^2\vec{v}+\mu\nabla\left(\nabla\cdot\vec{v}\right)+\vec{S}_{\mu}+\rho\vec{g}+\vec{S}_{\sigma}\right)dV, \tag{6}$$

in which all the terms that include the variation of the dynamic viscosity μ have been gathered into the source term $\vec{S}_{\mu}$. The additional momentum source term S_{σ} accounts for the surface tension, which is expressed according to the Continuum Surface Force model (CSF) [7] as

$$S_{\sigma}=\sigma\frac{\rho\kappa\nabla\gamma}{\frac{1}{2}\left(\rho_l+\rho_g\right)}. \tag{7}$$

The sum of forces acting on the differential volume dV should equate its acceleration, i.e. Newton's second law. Developing the material derivative of the linear momentum and considering the variation of the density one obtains

$$\frac{D\left(\rho\vec{v}\right)}{Dt}=\vec{v}\frac{D\rho}{Dt}+\rho\frac{D\vec{v}}{Dt}. \tag{8}$$

Equating Eqn. (6) to Eqn. (8) – and combining with Eqn. (5) – one obtains the following conservation equation

$$-\nabla p+\mu\nabla^2\vec{v}+\mu\nabla\left(\nabla\cdot\vec{v}\right)+\vec{S}_{\mu}+\rho\vec{g}+\vec{S}_{\sigma}=\vec{v}S_{mass}-\vec{v}\rho\left(\nabla\cdot\vec{v}\right)+\rho\frac{D\vec{v}}{Dt}, \tag{9}$$

in which p is the pressure, $\vec{g}$ is the acceleration of gravity, and the mass source term S_{mass} takes part of an additional momentum source. Therefore, analogously to what happens in a variable-mass system, the acceleration has one term caused by the variation of the velocity and another caused by the variation of mass.

The mass source term S_{mass} is implemented in the simulations using user-defined functions (UDFs). It is calculated adding the source term caused by the absorption and the source term S_i which describe the consumption/creation of reactants/products in the chemical reaction as

$$S_{mass}=Ek_lA_{eff}\Delta c+S_i, \tag{10}$$

being E the enhancement factor, Δc the concentration difference between the gas-liquid interface and the bulk of the liquid, and the effective area A_{eff} equals the modulus of the volume fraction gradient

$$A_{eff}=\left|\nabla\gamma\right|. \tag{11}$$

The liquid-side mass transfer coefficient k_l is, using Higbie's penetration theory:

$$k_l = 2\sqrt{\frac{D}{\pi\tau}}, \tag{12}$$

being D the diffusivity of the absorbed component into the liquid film, and the contact time τ is estimated as the quotient between the length of the liquid film – in the direction of the flow – and the velocity at the gas-liquid interface.

The enhancement factor E quantifies the increase on the absorption rate which occurs when there is a chemical reaction between the absorbent and the species being absorbed. The enhancement factor is approximated to the value of the Hatta number Ha, since the reaction between the carbon dioxide and the monoethanolamine (MEA)

$$CO_2 + MEA + H_2O \longleftrightarrow MEACOO^- + H_3O^+ \tag{13}$$

follows the pseudo-first order behavior and the proportion of MEA in the liquid phase exceeds the stoichiometric requirement [8]. The expression of the enhancement factor is thus

$$E \cong Ha = \sqrt{\frac{K_{for}\left[MEA\right]D}{k_l}}. \tag{14}$$

Also, the mass source term S_{mass} is proportional to the concentration difference between the gas-liquid interface c_{int} and the bulk of the liquid phase c_{bulk} of the component being absorbed:

$$\Delta c = c_{\text{int}} - c_{bulk}. \tag{15}$$

The concentration at the interface c_{int} is the solubility of the species being absorbed, which is calculated according to Penttilä et al [9]. In the case of MEA and carbon dioxide, the reaction is fast enough for the carbon dioxide to be consumed as soon as it penetrates into the liquid film. The concentration at the bulk of the liquid phase c_{bulk} can be neglected under those conditions, and therefore the concentration difference equals the solubility.

2.2. Verification of the model

A simple grid convergence study is performed in order to verify the model. The generalized Richardson extrapolation, which calculates the numerical solution Φ of a variable by adding a series of correction terms to the exact solution Φ_{exact}, is used for that purpose:

$$\Phi = \Phi_{exact} + g_1 h + g_2 h + h.o.t., \tag{16}$$

in which h is the grid spacing, g_a and g_b are functions that do not depend on the grid spacing, and h.o.t. stands for high order terms.

The grid convergence index GCI is calculated as

$$GCI = \frac{F_s\left|\varepsilon\right|}{r^p - 1}, \tag{17}$$

where r is the grid refinement ratio, the relative error ε is calculated as $\varepsilon = \left(\Phi_2 - \Phi_1\right)/\Phi_1$, and F_s is a factor of safety which has a value of 1.25 if three grids are used in the convergence study [10].

The order of convergence p is obtained by applying the following expression:

$$p = \frac{\ln\left(\frac{f_3 - f_2}{f_2 - f_1}\right)}{\ln(r)}, \tag{18}$$

in which the fine, medium and coarse grid are denoted with the subscripts 1, 2 and 3 respectively – this also applies to the above formula for the relative error ε.

Finally, one must check whether or not the results lie within the asymptotic range. Otherwise, the generalized Richardson extrapolation is not applicable.

$$\frac{GCI_{32}}{r^p GCI_{21}} \cong 1. \tag{19}$$

If the data meet the above condition, then one can estimate the extrapolated value at zero grid spacing as

$$\Phi_{extr} = \frac{r_{21}^p \Phi_1 - \Phi_2}{r_{21}^p - 1}. \tag{20}$$

However, convergence within the asymptotic range is not the only case which may occur. Divergence, convergence out of the asymptotic range and oscillatory convergence might appear as well. These three possibilities can be evaluated by applying the following expression

$$R = \frac{\Phi_2 - \Phi_1}{\Phi_3 - \Phi_2}, \tag{21}$$

which may give way to the following outcome:

- Monotonic convergence if $0 < R < 1$,
- Oscillatory convergence if $R < 0$,
- Divergence if $R > 1$

Uncertainty can still be assessed, when there is oscillatory convergence, as half of the difference between the upper and the lower value observed.

3. Results and discussion

3.1. Small-scale simulations

Simulations at small-scale have been used to study the reactive mass transfer between the gas and the liquid phase. A simple grid convergence study of the gas-liquid interface area – using a 3D computational domain – and the concentration of the absorbed species (CO_2) – in a 2D domain – has been conducted. Fig. 1 shows a schematic of the computational model at small-scale, with its relation with the actual structured packing. The boundary conditions and the direction of the coordinate axes are also depicted.

Fig. 2 shows the time evolution of the interface area for the liquid film formed over a metallic plate inclined 60° over the horizontal plane. The simulation has been run until no significant differences between two consecutive time steps appear, e.g. the maximum relative difference between the last two time steps is less than 0.45%. Table 1 shows the results of applying the generalized Richardson extrapolation to the interface area upon the specified conditions. One can observe that reasonable values of the uncertainty caused by the discretization are obtained. In addition, the results lie within the asymptotic range as it can be inferred from the application of the Eqn. (19), which gives a value

of 1.0024. One can conclude from these results that a grid spacing between 11 μm and 16 μm should be appropriate for modelling at small-scale. In addition, more grid convergence studies of the sort are needed in multiphase simulations. In effect, experimental data available for validation are scarce, hence conducting these studies can provide further confidence in CFD calculations.

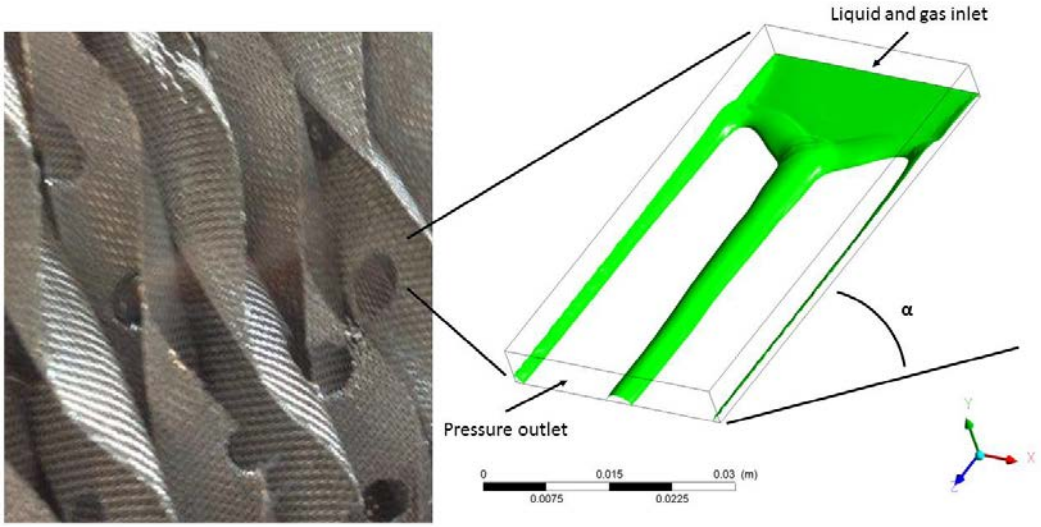

Fig. 1 Physical interpretation of the CFD model at small-scale. The image on the left hand side corresponds to a sample of SULZER CHEMTECH GEWEBEPACKUNG BX available at the University of Surrey. The image on the right hand side corresponds to the computational domain used at small-scale: an inclined metallic plate with an inclination α over the horizontal. The dimensions of the plate are (0.03 x 0.005 x 0.06) m. Note that rivulets and a front wave form instead of a perfectly developed liquid film. The liquid inlet is a 0.35 mm slot in the upper part of the domain.

Table 1 Grid convergence study of the interface area f .

Variable	Value
f_1	8.9723 cm^2
f_2	8.9073 cm^2
f_1	8.8777 cm^2
f_{extr}	8.8529 cm^2
p	4.3144
GCI_{21}	0.1420%
GCI_{32}	0.3108%
$GCI_{32}/r^p GCI_{21}$	1.0024

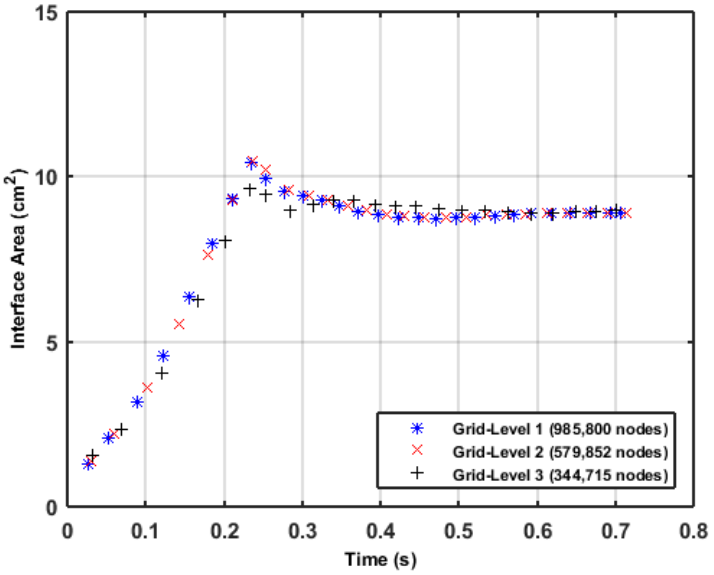

Fig. 2 Transient evolution of the gas-liquid interface area over the 3D computational domain shown in Fig. 1. The velocity of the liquid at the inlet is 26 cm/s. Air/water system. The gas phase is stagnant at atmospheric pressure The grid spacing in the liquid film thickness zone is 11.4 µm, 13.8 µm and 16.7 µm for Grid-Level 1, 2, and 3 respectively.

Grid convergence studies can be applied to either overall variables - such is the case of the interface area - or to variables calculated at particular grid points. As discussed above, small-scale simulations have been used to model the reactive mass transfer between the gas and the liquid phase. A simple grid discretization error assessment has been carried in a 2D domain (0.01 x 0.005) m, with 158,400 nodes. The gas phase is CO_2 whereas the liquid phase is a 30% wt aqueous MEA solution. The velocity at the liquid inlet is 27 cm/s. A constant value of the source term is implemented (92 kg/m^3/s). The results of the grid convergence with three grids are shown in Table 2, along with the correspondent values of the grid spacing. The mass fraction is taken in a grid point placed at 5 cm from the liquid inlet and 0.35 mm from the plate surface – the thickness of the liquid inlet slot.

Table 2 Grid convergence study of the CO_2 mass fraction C.

Variable	Value
C_1	0.002571
C_2	0.002484
C_3	0.002497
Uncertainty	0.0000431

The model was hereafter used to obtain the CO_2 concentration profiles within the liquid film. Fig. 3 shows the concentration profiles at the center of the domain for three aqueous amine concentrations. The results show that the CO_2 concentration is zero in the bulk of the liquid. This is caused by the fast kinetics of the chemical reaction, which results in the consumption of the absorbed species short after it crosses the interface. Furthermore, the plot shows lower values of the concentration as the proportion of amine in the solution increases. This can be explained by the fact that a greater amine contents in the solution gives rise to a faster chemical reaction, which eventually results in a smaller concentration of the reactants.

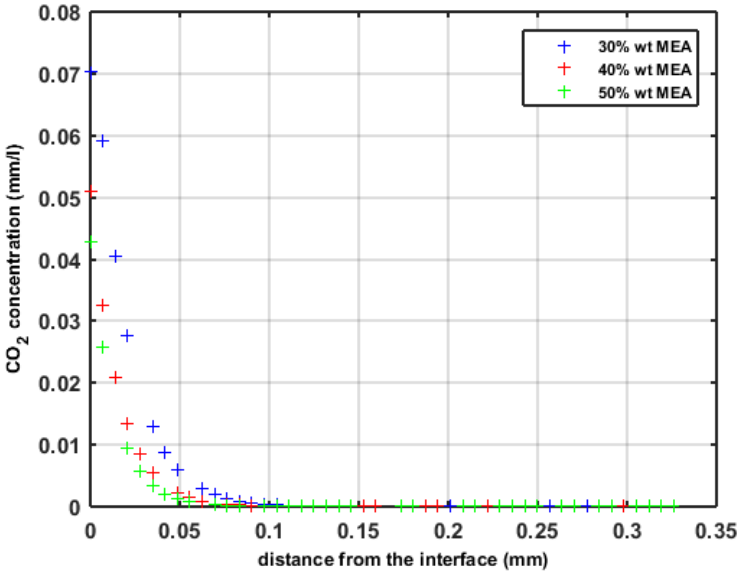

Fig. 3. CO_2 concentration vs distance from the interface. This profile corresponds to the centre of the domain, at 5 cm from the interface. The liquid inlet velocity is 2.5 cm/s. The gas is pure CO_2 at atmospheric pressure.

3.2. Meso-scale simulations

Further to the dry pressure drop, implementing interface tracking methods such as the VoF model in the simulations of the packing at meso-scale allows the CFD practitioner to obtain two parameters which are key to a good understanding of the flow inside the structured packing column: the liquid hold-up and the interface area.

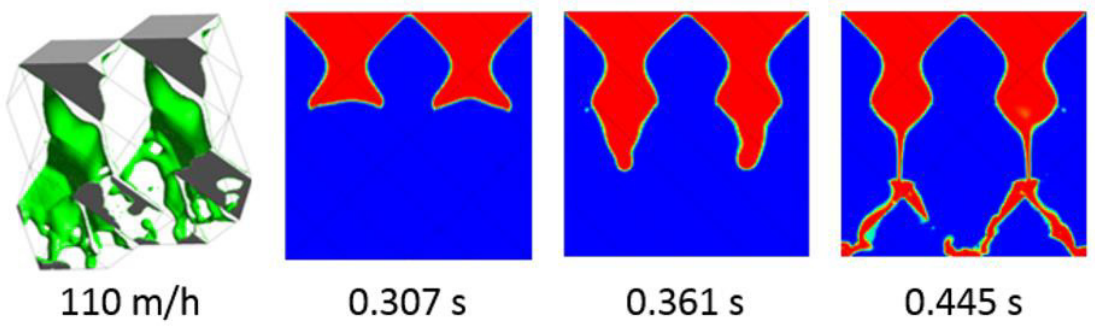

Fig. 4 Liquid phase development inside 4 REUs of the commercial packing MontzPak B1.250M. The image on the left hand side is an isometric view of the gas-liquid interface inside the packing. The liquid volume has been obtained considering that the interface is formed by those cells which have a value of the volume fraction of 0.5. The other three images are volume fraction maps on the middle plane (red denotes the liquid phase whereas dark blue denotes the gas) at different time steps. Air/water system with a liquid load of 110 m/h. The gas phase is stagnant at atmospheric pressure. The grid used in these calculations has 5,782,612 nodes.

Fig. 4 provides a glimpse of the liquid phase development inside the real geometry of the packing. A structured packing is formed by a repeating unit – called representative elementary unit (REU) in the literature. Since it has been reported in the literature that computational domains featuring a small number of those REUs are capable of capturing the dry pressure drop [11], this research aims at proving that such a CFD strategy can also predict both the liquid hold-up and the interface area.

The liquid hold-up is defined as the volume of liquid phase per unit volume of the packing. The liquid hold-up has a direct effect on the pressure drop of the column. In effect, the greater the amount of liquid which builds up inside the column, the greater the pressure drop per unit length. This is caused by the reduction on the space available for the gas to flow, that is to say, the reduction on the porosity of the packing, which causes the subsequent acceleration of the gas phase.

Fig. 5 shows the comparison between the data obtained with the present model and the experimental correlations found in the literature for the liquid hold-up. The liquid hold-up has been obtained from the simulations by creating a volume with those computational cells the volume fraction of which is between 1 and 0.5. The assumption of stagnant gas phase has been taken in the simulations, since the gas phase velocity does not affect the development of the liquid phase when the system is in the pre-loading region. To illustrate this, for a given liquid load there is a gas superficial velocity threshold before which the inertia of the gas does not affect the liquid flow (pre-loading region). Beyond that threshold, the gas begins to push the liquid toward the upper part of the column, which results in a greater liquid hold-up and therefore a greater pressure drop. The limit is reached when the gas flow totally impedes the liquid from flowing downwards, in which is called flooding. The normal operating conditions are pre-loading conditions. We assume in the present work that the column is operating at pre-loading conditions. Therefore, it would be legitimate to consider that the gas flow is stagnant.

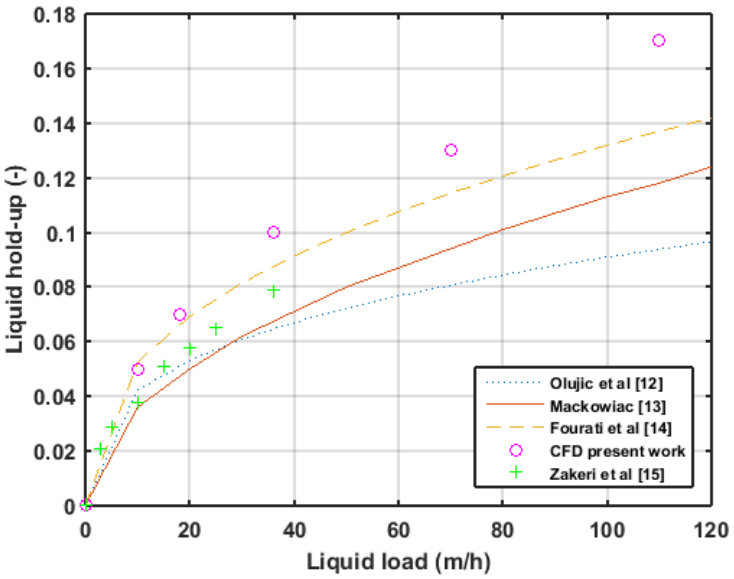

Fig. 5 Liquid hold-up vs liquid load. Comparison between CFD simulations and experimental data for air and water. The values of the liquid load considered in this study encompass the experimental range of values found in the literature, which can only adopt values up to 120 $m^3/m^2/h$ because of the size of experimental rigs. In industrial applications, the liquid load can have values up to 240 $m^3/m^2/h$. The contact angle is 70° (water on a steel surface). MontzPak B1.250M.

One can see in the plot that the liquid hold-up is overestimated by the CFD model. However, the value of the liquid hold-up can vary significantly depending on which point within the column is considered. As reported by Olujić et al [12], the liquid hold-up has been usually estimated as the product of the thickness of the liquid film

times the specific area, i.e. the area of the packing per unit volume. Such a calculation is based on the assumption that a completely developed liquid film covers the entire surface of the packing. However, in practice, such conditions are never reached, because liquid formations as droplets and rivulets along with accumulations on dead zones appear instead as can be seen in Fig. 4. Despite being an ideal case, one can see in the Fig. 5 that the values predicted under the assumption of the perfectly developed liquid film give rise to a liquid load prediction within the same order of magnitude as the rest of experimental data. The general tendency of the relationship between both variables is reproduced by the present CFD model, with a greater rate of growth at low values of the liquid load than at greater ones. One can also observe that the difference between the series of data tends to diminish with the liquid load.

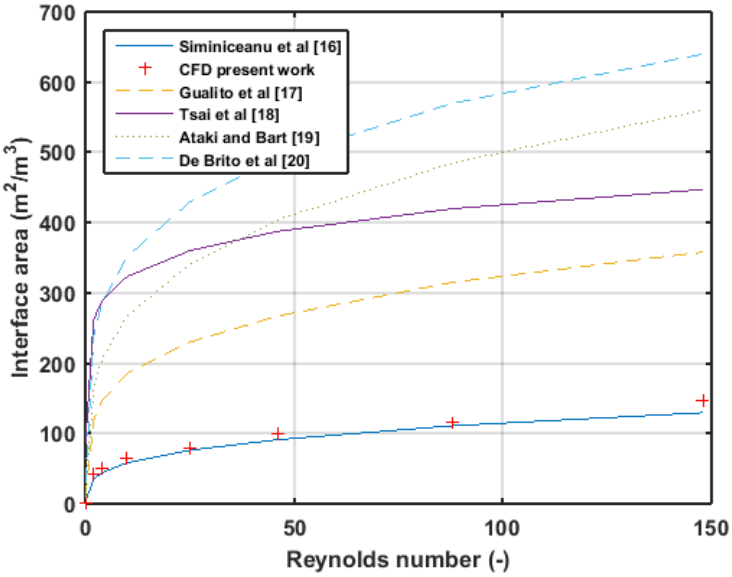

Fig. 6 Interface area vs Reynolds number. Comparison between CFD simulations and experimental data for air and water. . The contact angle is 70° (water on a steel surface). MontzPak B1.250M.

Fig. 6 shows the comparison between the interface area predicted by the present CFD work and experimental correlations as a function of the Reynolds number. The latter has been selected in this instance instead of the liquid load to compare against the experimental correlations found in the literature. Nevertheless, only the velocity at the liquid inlet has been changed in the simulations whilst the rest of the parameters in the Reynolds number were kept constant. Under those circumstances, the Reynolds number can be seen as a measure of the liquid velocity, too. The Reynolds number is calculated using the liquid inlet velocity and its correspondent liquid film thickness according to Nusselt's theory [21].

As in the case of the liquid hold-up, Fig. 6 also shows a huge difference between the correlations. However, the shape of the curve is reproduced correctly by the present simulations. The graph shows a greater rate of growth for low values of the Reynolds number, whereas the curve tends to level off as the Reynolds number increases.

Thereafter, the model has been used to assess the effect of the surface tension on both the interface area and the liquid load. Fig. 7 and Fig. 8 show the effect of the surface tension on the transient development of both the liquid hold-up and the interface area respectively. The simulations are run until small variations on the liquid hold-up appear. According to the results, it would be interesting to reduce the surface tension so as to keep the liquid hold-up to a minimum and maximize the interface area available for mass transfer. This conclusion is in accordance with the results found in the literature, according to which, increasing the Weber number results in a better liquid spreading [22].

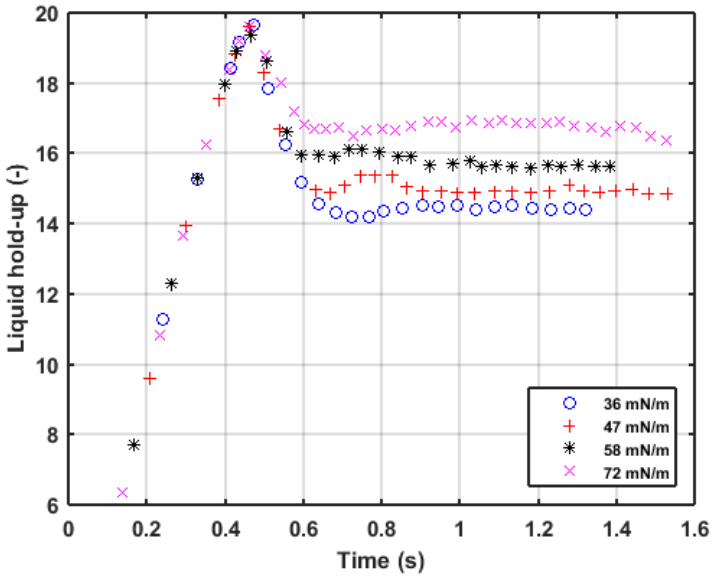

Fig. 7 Transient behaviour of the effect of the surface tension on the liquid hold-up at meso-scale. Air/water system. 110 m/h liquid load. MontzPak B1.250M.

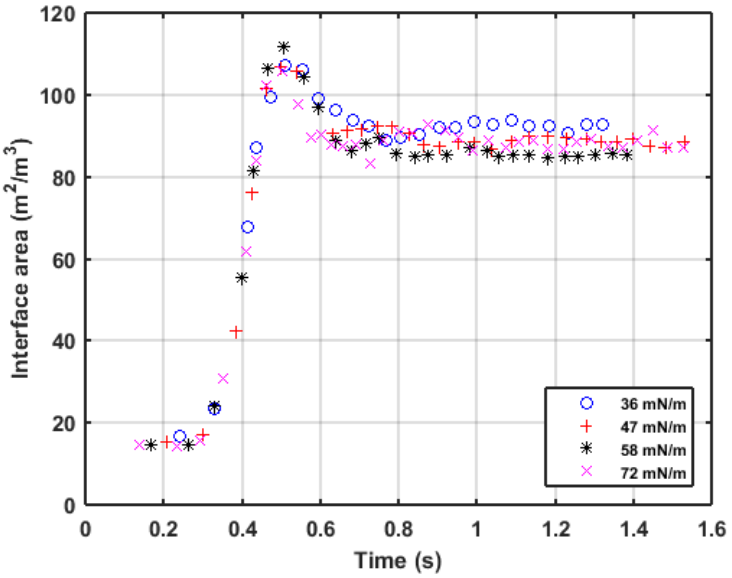

Fig. 8 Transient behaviour of the effect of the surface tension on the interface area available for mass transfer at meso-scale. Air/water system. 110 m/h liquid load. MontzPak B1.250M.

4. Conclusions and future work

A CFD model to describe the hydrodynamics in structured packing columns for Carbon Capture and Storage has been developed. CFD models with this purpose are split in three scales: small-, meso- and large-scale in the literature. The present article introduces a CFD model of the packing at small- and meso-scale, and discusses its capabilities in terms of reactive absorption, liquid hold-up and interface area.

At the theoretical level, the Navier-Stokes equations for this particular application are derived, showing that both the continuity and the momentum equation can be combined into a single expression which governs the model. One can see that under the circumstances considered, the mass source term appears – combined with the velocity – as an additional momentum source term. Thus, the equation shows that the acceleration is the result of adding two terms: one caused by the velocity variation and another caused by the mass variation – analogously to what occurs in any mass-variable system.

Thereafter, a simple grid convergence study is carried out using the generalized Richardson extrapolation, followed by the discussion of the results at small-scale. One can observe that the model is able to reproduce the occurrence of the chemical reaction only at the interface, due to its fast kinetics.

Finally, the capabilities of the model at meso-scale are shown. The interface tracking allows the CFD user to reproduce the liquid hold-up and the interface area. The results from the simulations have been compared against various experimental correlations reported in the literature.

As a practical application of the model, further simulations are carried out to assess with the purpose of optimizing both the pressure drop and the interface area. In particular, the effect of the surface tension has been studied, with the purpose of improving the performance of the packing.

In summary, the present model can be used for improving geometries and solvents, or to develop new ones.

Acknowledgements

The authors gratefully acknowledge the financial support for this work by the UK Engineering and Physical Sciences Research Council (EPSRC) project grant: EP/J020184/1 and FP7 Marie Curie iComFluid project grant: 312261.

References

[1] Hester RE, Harrison RM. Carbon Capture Sequestration and Storage. Cambridge: The Royal Society of Chemistry; 2010.
[2] Ansolabehere S, Deutch J, Driscoll M, Gray PE, Holdren JP, Joskow PL, Lester RK, Moniz EJ, Todreas NE. The future of nuclear power. Cambridge (MA): Massachusetts Institute of Technology; 2003.
[3] OECD Factbook 2009: Economic, Environmental and Social Statistics. OECD; 2009.
[4] Raynal L, Royon-Lebeaud A. A multi-scale approach for CFD calculations of gas-liquid flow within large size column equipped with structured packing. Chem Eng Sci 2007;62:7196–7204.
[5] Fernandes J, Lisboa PF, Simões PC, Mota JPB, Saatdjian E. Application of CFD in the study of supercritical fluid extraction with structured packing: wet pressure drop calculations. J Supercrit Fluids 2009;50:61–68.
[6] Kim J, Pham DA, Lim YI. Gas-liquid multiphase computational fluid dynamics (CFD) of amine absorption column with structured packing for CO_2 capture. Comput Chem Eng 2016; 88:39–49.
[7] Brackbill JU, Kothe DB, Zemach C. A continuum method for modelling surface tension. J Comput Phys 1992;100:335–354.
[8] Wilcox J, Rochana P, Kirchofer A, Glatz G, He J. Revisiting film theory to consider approaches for enhanced solvent-process design for carbon capture. Energy Environ Sci 2014,7:1769–1785.
[9] Penttilä A, Dell'Era C, Uusi-Kyyny P, Alopaeus V. The Henry's law constant of N_2O and CO_2 in aqueous solutions (MEA, DEA, DIPA, MDEA, and AMP). Fluid Phase Equilib 2011;311:59–66.
[10] Roache P. Verification and validation in computational science and engineering. Albuquerque (NM): Hermosa; 1998.
[11] Armstrong LM, Gu S, Luo KH. Dry pressure drop prediction within Montz-Pak B1-250.45 packing with varied inclination angles and geometries. Ind Eng Chem Res 2013;52:4372–4378.
[12] Olujić Ž, Jansen H, Kaibel B, Rietfort T, Zich E. Stretching the capacity of structured packings. Ind Eng Chem Res 2001;40:6172–6180.
[13] Maćkowiac J. Pressure drop in irrigated packed columns. Chem Eng Process. 1991;29:93–105.
[14] Fourati M, Roig V, Raynal L. Experimental study of liquid spreading in structured packings. Chem Eng Sci 2012;80:1–15.
[15] Zakeri A, Einbu A, Svendsen HF. Experimental investigation of liquid holdup in structured packings. Chem Eng Res Des 2012;90:585–590.

[16] Siminiceanu I, Friedl A, Dragan M. A simple equation for the effective mass transfer area of the Mellapak750Y structured packing. Conference proceedings of the Scientific Conference Meeting *"35 Years of Petroleum-Gas University Activity"*, Ploieşti, Romania, 2002.
[17] Gualito JJ, Cerino FJ, Cardenas JC, Rocha JA. Design method for distillation columns filled with metallic, ceramic or plastic structured packings. Ind Eng Chem Res 1997;36:1747–1757.
[18] Tsai RE, Seibert AF, Eldridge RB, Rochelle GT. Influence of viscosity and surface tension on the effective mass transfer area of structured packing. Energy Procedia 2009;1:1197–1204.
[19] Ataki A, Bart HJ. Experimental and CFD simulation study for the wetting of a structured packing element with liquids. Chem Eng Technol 2006;29:336–347.
[20] De Brito MH, von Stockar U, Bangerter AM, Bomio P, Laso M. Effective mass-transfer area in a pilot plant column equipped with structured packings and ceramic rings. Ind Eng Chem Res 1994;33:647–656.
[21] Nusselt W. Die Oberflächenkondensation des Wasserdampfes. Zeitschrift des Vereines Deutscher Ingenieure 1916;60:541–546.
[22] Hoffmann A, Ausner I, Repke JU, Wozny G. Detailed investigation of multiphase (gas-liquid and gas-liquid-liquid) flow behavior on inclined plates. Chem Eng Res Des 2006;84:147–154.